EXPERIMENTAL STUDIES OF VORTEX FLAPS AND VORTEX PLATES

K. Rinoie* and J.L. Stollery

College of Aeronautics, Cranfield Institute of Technology
Cranfield, Bedford, MK43 0AL, U.K.

Abstract

Low-speed wind tunnel tests have been made on a number of vortex flap and vortex plate configurations, in order to assess the benefits of these devices. The force and surface pressure measurements were made on a 1.15m span 60° delta wing model. Results indicate that the vortex flap deflection angle which causes the flow to come almost smoothly onto the flap surface without any large separation, shows a much higher lift/drag ratio than the flap deflection angle which forms a leading-edge separation vortex over the flap surface. The performance of a vortex plate protruding from the leading-edge of the datum delta wing is comparable to that of the vortex flap. However, when the vortex plate is used with the vortex flap deflected, it showed no benefit in these tests.

Nomenclature

b	Local span
C_r	Wing centre-line chord
C_D	Drag coefficient
C_{D0}	C_D at zero lift
C_L	Lift coefficient
C_m	Pitching moment coefficient non-dimensionalised using C_r and measured about $x/C_r = 0.4$
C_p	Pressure coefficient
g	Vortex plate leading-edge position measured from leading-edge of the wing in the chordwise direction
L/D	Lift/Drag ratio
Re_{C_r}	Reynolds number based on wing centre-line chord
x	Chordwise co-ordinate measured from the apex of the delta wing
y	Spanwise co-ordinate orthogonal to x, measured from the wing centre-line
α	Wing incidence
α_g	Geometrical wing incidence (i.e. without tunnel corrections)
δ_f	Vortex flap deflection angle measured normal to the hinge line

I. Introduction

The leading-edge vortex flap (LEVF) is a full span deflectable surface at the leading-edge of a delta wing (ref.1). With the flap deflected downward, a leading-edge separation vortex may be formed over the forward facing flap surface (fig.1). The suction force generated by the vortex acts on the flap surface and generates a thrust component. Hence the drag is reduced and the lift/drag (L/D) ratio improved. This L/D ratio is an essential factor for the take off and climb performance of delta wing aircraft. Many tests have been made and confirm that the LEVF can improve the low speed aerodynamic efficiency of delta wings. Ref.2 gives an overview of LEVF research.

Some earlier tests using a 60° delta wing model with tapered vortex flaps were made at the College of Aeronautics (ref.3). They showed that the LEVF can increase the L/D ratio by up to 40%, and the L/D ratio is improved over a large range of lift coefficients with little change of trim. It was suggested in ref.3 that the optimum L/D ratio is achieved with the flow coming smoothly onto the deflected LEVF without forming a vortex above or below the flap surface.

The vortex plate proposed in ref.4 is similar to a forward facing split flap. This vortex plate is a thin plate attached to the lower surface of the leading-edge of the delta wing (fig.2a). With the plate fitted, a leading-edge cavity is formed between the delta wing and the vortex plate. Ref.4 suggested that at positive incidence the flow separates at the plate leading-edge and forms a spanwise vortex which induces a suction over the cavity surface. Hence the plate creates some leading-edge thrust and the drag is reduced.

In order to investigate the flow around the LEVF at the maximum L/D condition and to understand how the vortex plate works, a pilot study (ref.5) was made using a 0.53m span 60° flat delta wing fitted with vortex flaps and vortex plates. The results are summarised below:

a) At the incidence when the L/D ratio reaches a maximum, the flow comes nearly smoothly onto the flap with no large vortex being formed, as was suggested in ref.3.
b) At high incidences a leading-edge separation vortex is formed on the LEVF surface. Because of the suction effect of this vortex, the L/D is higher than that of the datum wing, as was suggested in ref.1.
c) By fitting a vortex plate to the basic wing (no LEVF), the L/D ratio for all ranges of C_L greater than 0.3 is significantly improved. A better performance was obtained with the vortex plate protruding ahead of the leading-edge of the wing (fig.2b).

These previous studies (refs.3 and 5) concentrated on incidences up to about 30° because the emphasis was on finding the maximum L/D ratios. These values occurred at rather low lift coefficients. Ref.3 showed that the LEVF was still giving some L/D improvement at the highest incidence tested. In practice any benefit at high incidence may be useful.

* Permanent Address:
National Aerospace Laboratory, 7-44-1 Jindaiji-higashi-machi, Chofu, Tokyo, 182, Japan

In ref.5 the vortex plate was attached to the delta wing without flaps deflected. However, when the vortex plate is attached to the deflected vortex flap as is shown in fig.2c, the drag reduction will be caused by the effect of combining the vortex flap and the vortex plate. There may be some beneficial effects on wing performance.

In the present study, further tests were conducted. The purpose of this study is
1) to gain more understanding of the complex flows around the delta wing with vortex flaps up to incidences of 60°,
2) to confirm the flow conditions giving the maximum L/D ratio of the wing with vortex flaps,
3) to investigate the benefits of the vortex plate, with and without flaps deflected.

II. Experimental Details

Fig.3 shows the model details. This model is the same one that was used in ref.3. The model is a 60° delta wing with sharp leading-edge and trailing-edges. The centre-line chord length Cr is 1.0m. The aerofoil section at centre line is a symmetrical smooth convex shape described by the form:

$$\frac{y}{Cr} = \pm\frac{x}{8Cr}\left(1-\frac{x}{Cr}\right)\left(1-\frac{x}{2Cr}\right)$$

The maximum thickness/chord ratio is 4.8%. The spanwise thickness distribution varies linearly from centre-line to tip. The model has the LEVF hinge lines running from the wing apex to 75% of the trailing-edge semispan station. Two rows of pressure tappings were located on the upper surface.

The flap deflection angle δ_f is defined as the angle measured in the plane normal to the hinge line. Different flap deflections of $\delta_f = 0°$ to 60° were tested in ref.3. It was concluded that the $\delta_f = 30°$ case has the best performance for a wide C_L range. In order to check the repeatability of measurements in ref.3 and in order to measure the flap performance at high incidences greater than 30°, the datum wing ($\delta_f = 0°$) and $\delta_f = 30°$ cases were again tested here. Nine different flap deflections of $\delta_f = 0°$ to 60° were tested to determine the maximum L/D condition for each flap setting.

Two different types of vortex plate were tested in this experiment. The first type (fig.4a) is a similar to the one used in ref. 5. The plate was attached to the lower surface of the datum model (no LEVF deflection). The plate was bent as shown in fig.4a so that the distance between the leading-edge of the plate and that of the wing was 10mm at every spanwise station in side view. The plate can be moved forward, as shown in fig.4a. The position of the plate is defined by the chordwise distance (g) between the leading-edge of the wing and that of the vortex plate. In these tests the plate was set at $g/Cr = 0$ and 0.02. The vortex plate described above is called the "parallel" vortex plate.

A second type of vortex plate was made in order to check the effect combining the vortex plate and the vortex flap. The plan shape is smaller than the vortex flap as is shown in fig.4b, so that the vortex flap is deflectable. The distance between the leading-edge of the plate and that of the wing in side view is 10mm at the trailing-edge of the wing. This distance decreases linearly towards the apex of the wing. At the apex this distance is zero. The leading-edge of the plate coincides with that of the wing in plan view. The measurements were done without flaps deflected ($\delta_f = 0°$) and with a flap deflection angle (δ_f) of 30°. This vortex plate is hereafter referred to as the "tapered" vortex plate.

The experiments were made in the Cranfield 2.4m x 1.8m low speed, closed working section, closed return wind tunnel. All tests were done at a tunnel speed of U_∞ = 30m/s. The Reynolds number based on the wing centre line chord was 2×10^6. The model was mounted inverted from the overhead balance by a single shielded strut and a tail wire. For measurements over the incidence range of -8° to 32°, the model was mounted at the centre line of the tunnel. However, it was impossible to set the model at an incidence above 45° in this way. Therefore, an extended centre strut and an extended curved tail strut were used for measurements in the incidence range of 30° to 57°.

Lift, drag and pitching moments were measured using the overhead 6-component electro-mechanical balance. Tunnel boundary corrections were applied to the measured data. Interference between the strut and the model was not accounted for. Since the tunnel boundary corrections used here are only suitable for low incidences, the results obtained here at high incidences must be treated with caution. All aerodynamic coefficients were calculated based on the constant datum delta wing area. In order to measure surface pressure distributions, a "Scanivalve" was mounted within the model. Further experimental details can be found in ref.6.

III. Results and Discussion

Vortex Flap

Fig. 5 shows the C_L vs. α curves for the datum wing and the $\delta_f = 30°$ case. Results which were obtained using the low incidence rig and the high incidence rig are shown in the same figure. The two sets of results connect 'smoothly' at about α = 30°. At zero incidence, the C_L of the datum wing is slightly negative. Since the model is symmetrical the C_L should be zero. The reason why the C_L showed a negative value at α = 0° is thought to be due to the presence of the shielded strut. Fig.5 shows that deflecting the LEVF downwards moves the whole C_L-α curve to the right. Thus the zero lift incidence and the stall angle are increased while the C_L at a constant incidence (below the stall) is reduced.

In fig.5, a comparison is made with other experimental results from tests on a flat delta wing. In ref.7, measurements were made using a 0.92m span 60° delta wing at a Reynolds number of 2.37 million. This model had a 12% biconvex section, which is quite similar in shape to that of the present model. The results from the 12% biconvex wing tests are very similar to those of the datum wing tested here.

The C_D-α curves (fig.6) show the same trend, the whole curve being moved to higher values of incidence. The 12% biconvex wing (ref.7) shows larger C_D values than the present results at low incidences but this difference is reversed at the higher incidences. Drag is known to be sensitive to the section profile.

Fig.7 shows the lift to drag ratio (L/D) versus C_L. The $(L/D)_{max}$ for a flap deflection of 30° is increased

from the datum wing value of 10.4 to 11.3. For the datum wing, the L/D at negative lift is higher than that for positive lift. Again any lack of symmetry is probably due to strut interference. A large L/D improvement for $\delta_f = 30^\circ$ is seen at about $C_L = 0.25 \sim 0.5$. However, after the stall the $\delta_f = 30^\circ$ tests show that there is no benefit in using a LEVF.

Fig.8 shows the pitching moment curves measured about the model mounting point $x/C_r = 0.4$ for all tests including the vortex plate results. The LEVF has little effect on C_m. The $C_m - C_L$ curves are roughly linear before the stall. The C_m values at $C_L = 0$ are zero for the datum and the $\delta_f = 30^\circ$ cases. The aerodynamic centre position measured from the $C_m - C_L$ slope is $0.57C_r$.

These present results (figs.5–7) and the previous results in ref.3 (which were made at incidences up to 30°) agree well.

Fig.9 shows surface pressure distributions for the upper surface, for the datum and the $\delta_f = 30^\circ$ cases. Measurements were made at $x/C_r = 0.4$ and 0.8. Results at $x/C_r = 0.8$ were similar to those at $x/C_r = 0.4$, apart from low suction peaks at high incidences which were caused by vortex breakdown. Only the $x/C_r = 0.4$ results are shown in this paper.

Fig.9a shows that C_p distributions for the datum wing. At $\alpha = 6.2^\circ$ the features of a leading-edge separation vortex are clearly recognisable. There is a flat C_p area at the tip of the wing which shows the existence of a secondary separated flow. At $\alpha = 12.4^\circ$, 18.7° and 24.9° there is a large leading-edge separation vortex on the wing with high peak suctions. By $\alpha = 37.0^\circ$ the C_p distribution shows that the vortex suction has decreased but spread out to cover half the local wing span. This may signify vortex breakdown. At $\alpha = 48.7^\circ$, the C_p distribution is completely flat. This suggests that the vortex type of flow has collapsed and that the flow is now totally separated over the top surface of the wing.

Fig.9b shows the C_p distributions for the wing with $\delta_f = 30^\circ$. At $\alpha = 6.1^\circ$, there is no sign of vortex formation and this suggests that the flow comes smoothly onto the flap surface. At $\alpha = 12.3^\circ$, a separation region is seen on the flap. Although there is no sign of secondary separation, the suction measured in this region indicates the presence of a separation vortex. The spanwise length of this vortex at $\alpha = 12.3^\circ$ is almost the same as the flap span. At $\alpha = 18.6^\circ$, there are signs of a secondary separation inside the leading-edge separation vortex. At $\alpha = 24.8^\circ$, the suction caused by the vortex reaches its maximum value. After the stall ($\alpha > 37.1^\circ$), the C_p shows a flat distribution suggesting that the flow has totally separated from the wing surface. Therefore there was no benefit in L/D results for the $\delta_f = 30^\circ$ case after stall (fig.7).

The Effect of δ_f on L/D at Constant Incidence

In order to find the condition which gives the maximum L/D, some measurements were made by changing the flap deflection angle δ_f at constant incidence. Flap angles were varied between 0° and 60° at fixed incidence values of 6°, 8°, 10°, 12° and 14°. Force measurements and surface pressure measurements were made under these conditions. The incidences, as corrected for tunnel wall interference, are different for every flap deflection angle. Therefore, the geometrical incidence α_g as measured from the tunnel centre line is used in this section to define the incidence angle.

Fig.10 shows L/D versus δ_f at different incidences. This shows that at $\alpha_g = 6^\circ$ the L/D attains a maximum with $\delta_f = 20^\circ$. As the incidence increases, the maximum L/D decreases and the δ_f at which $(L/D)_{max}$ is achieved increases.

Fig.11 shows the measured pressure distributions for $\alpha_g = 6^\circ$ and 12° at $x/C_r = 0.4$. Different δ_f results (at constant α_g) are shown in each figure. At $\alpha_g = 6^\circ$ (fig.11a), the L/D attains its maximum at $\delta_f = 20^\circ$. At this flap deflection angle there is a small suction region at the leading-edge of the upper surface. On the lower flap surface at $\delta_f = 20^\circ$ there is no separation. At $\delta_f = 25^\circ$, there is no separation region on either surface. At $\alpha_g = 6^\circ$, as the flap deflection angle δ_f decreases below $\delta_f = 20^\circ$, so the spanwise length of the separation bubble on the top surface increases. At $\delta_f = 0^\circ$ there is a sign of secondary separation on the upper surface and a leading-edge separation vortex has formed over the wing. As δ_f increases beyond 20°, so separation occurs at the flap hinge line and a separation region is formed inboard of that line (see e.g. $\delta_f > 40^\circ$).

At $\alpha_g = 12^\circ$ (fig.11b), the L/D attains its maximum at $\delta_f = 30^\circ$. At this flap deflection angle the leading-edge separation vortex is formed on the flap upper surface and its reattachment line almost coincides with the flap hinge line (as was also shown in fig.9b). As δ_f decreases below $\delta_f = 30^\circ$, the spanwise length of the separation vortex increases as it did at the lower incidence ($\alpha_g = 6^\circ$). As δ_f increases above $\delta_f = 30^\circ$, the separation region is formed not only on the flap surface, but also inboard of the flap hinge line (e.g. $\delta_f = 40^\circ$). At $\delta_f = 60^\circ$, the vortex on the flap surface disappears and the only vortex formed is inboard of the flap hinge line.

Fig.12 shows C_D vs. C_L curves at constant incidence ($\alpha_g = 6^\circ$ and 12°) together with the corresponding flow pattern sketches in the transverse plane at $x/C_r = 0.4$. These flow pattern sketches were deduced from the pressure measurements. The C_D vs. C_L curves show that the C_L increases as the δ_f decreases at constant incidence and that the L/D ratio attains its maximum near the point where C_D is a minimum.

At the smaller incidence ($\alpha_g = 6^\circ$ the left hand curve of fig.12), when the flap deflection angle is zero ($\delta_f = 0^\circ$), a large leading-edge separation vortex is formed on the flap surface. Because of the suction effect of this vortex the C_D has a large value. At a flap deflection angle of 20° only a small separation bubble is formed on the flap and at $\delta_f = 25^\circ$ no bubble is formed at all. Since the flow comes almost smoothly onto the flap, the C_D has a much smaller value than that at $\delta_f = 0^\circ$. Further increase of δ_f causes the flow to separate at the flap hinge line and a separated region is formed inboard of the hinge line ($\delta_f = 40^\circ$ and 60° at $\alpha_g = 6^\circ$). Primarily because of this separated region inboard of the hinge line, the C_D of the $\delta_f = 40^\circ$ and 60° configurations have greater values than those of the $\delta_f = 20^\circ$ and 25° cases.

At the larger incidence of 12° (the right hand curve of fig.12), for both small δ_f ($\delta_f = 15°$) and large δ_f ($\delta_f = 60°$), the flow is similar to the patterns drawn for $\alpha_g = 6°$. However, when the L/D attains its maximum value ($\delta_f = 30°$), the leading-edge separation vortex is formed entirely over the flap surface and the flow reattaches near the flap hinge line. Because the vortex is formed only on the LEVF surface and the suction force of this vortex acts perpendicular to the deflected flap, the C_D shows a smaller value than those at other δ_f smaller than 30°, as was explained in section 1.

The $(L/D)_{max}$ at $\alpha_g = 6°$ is larger than that at $\alpha_g = 12°$, as was shown in fig.10. This implies that the highest L/D is attained when the flow comes smoothly onto the flap surface. A similar conclusion was reached in ref.5 where the wing model has a different cross section (bevelled edges) to the present model. This highest L/D ratio is reached at a small value of C_L. If a larger C_L is needed from a given configuration then a larger incidence is needed and the best L/D that can be achieved appears to be with the leading-edge vortex entirely on the flap and reattachment near the hinge line.

Vortex Plate

Fig.13 shows the C_L vs. α curves for parallel and tapered vortex plates together with the datum wing and the $\delta_f = 30°$ tests. In this section, the results of the vortex plate tests in the figures are not connected by lines in order to distinguish them from the results of the datum wing and $\delta_f = 30°$ results. This shows that the effects of either the parallel or the tapered vortex plates on lift are quite small.

Fig.14 shows the C_D vs. α curves. At incidences greater than 8°, the drag with the parallel vortex plate fitted (fig.14a) is smaller than the datum wing. The drag of the tapered vortex plate without LEVF deflection (fig.14b) is smaller than that of the datum wing. The drag of the tapered vortex plate with $\delta_f = 30°$ is smaller than that of the LEVF alone ($\delta_f = 30°$).The drag reductions of the tapered vortex plates are most significant at the higher incidences.

Fig.15 shows the L/D ratio vs. C_L. For the case of the parallel vortex plate with $g/Cr = 0$ (fig.15a), although the maximum value of L/D is reduced in comparison with the datum wing, the L/D ratio is improved for all C_L values greater than 0.4. For the case of the parallel vortex plate with $g/Cr = 0.02$ (fig.15a), the maximum value of L/D is almost the same as that of the datum wing, but it is achieved at a larger value of C_L. The L/D ratio is better with the vortex plate fitted for all values of C_L greater than 0.2. In comparison with the LEVF results, the L/D for $g/Cr = 0.02$ is roughly similar to that of the $\delta_f = 30°$ at positive C_L, although the maximum value is somewhat smaller (fig.7). For the tapered vortex plate without LEVF deflection (fig.15b), the maximum value of L/D is smaller than that of the datum wing. The L/D ratio is slightly improved for C_L values greater than 0.3 when compared with results for the datum wing. This is caused by the drag reduction as was seen in fig.14. For the tapered vortex plate with $\delta_f = 30°$ (fig.15b), there is no benefit at any C_L value.

The C_m distributions for parallel and tapered vortex plates in fig.8 show that the parallel and tapered vortex plates have little effect on C_m, as was found for the LEVF.

Figs.16a) and b) show surface pressure distributions for the upper surface of the parallel vortex plate ($g/Cr = 0.02$) and that of the tapered vortex plate with $\delta_f = 30°$ at $x/Cr = 0.4$. Fig.16a shows that there is only a small separation region at $\alpha = 6.2°$ on the wing, although a leading-edge separation vortex is formed on the datum wing at the same incidence as was shown in fig.9a. Increasing the incidence to 12.4°, there is a leading-edge separation vortex on the wing, but the spanwise length of this vortex is about 10% shorter than that on the datum wing at the same incidence (fig.9a) and there is no sign of secondary separation. These results suggest that onset of the leading-edge separation vortex is delayed by the vortex plate $g/Cr = 0.02$. Fig.16b shows Cp distributions for the tapered vortex plate with $\delta_f = 30°$. It is seen that the spanwise length of the leading-edge separation vortex at incidences 12.3° and 18.5° is shorter than that of the $\delta_f = 30°$ case at the same incidences (fig.9b).

Leading Edge Suction

In this section, the leading-edge suctions recoverable through vortex flap and vortex plate deployments are discussed. The drag of a flat plate wing with no leading-edge suction is:

$$C_D = C_{DO} + C_L \tan\alpha ,$$

where C_{DO} is the zero-lift drag coefficient which depends on the surface skin friction and the form drag. Using the measured C_L and C_{DO}, C_D assuming 0% leading-edge suction is calculated from the above formula and is plotted on the C_D vs. C_L curves together with the measured data in figs 17a-d. In order to plot the 0% leading-edge suction curves, $dC_L/d\alpha$ was assumed to be equal to the measured value.

In contrast, a wing with a well rounded leading-edge can show a large drag reduction due to leading-edge suction. In order to give some idea of the magnitude of this leading-edge suction, experimental data taken from ref.8 for a wing with a well rounded leading-edge are also plotted (figs.17a and b). In ref.8, measurements were made using a 0.91m span 60° delta wing which had a 10% thickness ratio aerofoil section at a Reynolds number of 18.6 million (based on the root chord). The nose radius was 0.69% of the chord length.

Fig.17a shows the results for our datum wing. The measured drag polar shows almost the same value as that of the 0% leading-edge suction estimate at all incidences. This confirms that the datum wing with a sharp leading-edge develops no leading-edge suction force.

Fig.17b shows the drag results for the wing with the LEVF deflected 30°. The measured value is considerably less than that estimated assuming zero leading-edge suction, for all incidences. When compared with the rounded leading-edge data (ref.8), it can be seen that the vortex flap achieves a significant amount of C_D reduction.

The results for the parallel vortex plate $g/Cr = 0.02$ (fig.17c) show that the measured drag value is less than that for the zero leading-edge suction estimate at all positive incidences. This means that some leading-edge

suction is recovered by incorporating a vortex plate. It is not clear that this C_D reduction is caused by the suction effect of a separation vortex between the leading-edge of the wing and that of the vortex plate as was suggested in ref.4. Smoke visualization tests, made on a different model with vortex plates in ref.5, did not confirm the existence of this vortex. It may be that the suction force is produced by the separated flow acting on the forward facing region between the wing and the vortex plate. Because of this, the C_D is reduced (as was shown in fig.14) and the L/D improved for C_L values greater than 0.2 (as was shown in fig.15).

The decrease in L/D ratio for small values of C_L (fig.15) is probably due to differences in the values of C_{Do}. The C_{Do} of the parallel vortex plate configuration is larger than that of the datum wing, because of the difference of the forward facing area. Since a small increase in C_D causes a large decrease in L/D ratio at low values of C_L, the result is a reduction in the L/D values for the wing fitted with parallel vortex plates, as shown in fig.15.

When compared with the results of the tapered vortex plate with 30° LEVF deflection (fig.17d) and those of the LEVF alone (fig.17b), the C_D reduction is almost the same. The vertical distance between the leading-edge of the wing and the vortex plate is 10mm as measured at the wing tip. This is the same as for the parallel vortex plate. However this gap decreases towards the apex as shown in fig.4. Therefore, the total forward facing area between the tapered vortex plate and the wing is smaller than that for the parallel vortex plate. The leading-edge suction acting on a smaller area gives a smaller drag reduction. Furthermore, the C_{Do} is larger than that of the LEVF ($\delta_f = 30°$) alone. The result is that the maximum L/D of the tapered vortex plate with $\delta_f = 30°$ is smaller than that of the LEVF alone as seen in fig.15.

IV. Conclusions

1) The improvements in lift/drag ratio obtained by deflecting a leading-edge vortex flap (as reported in ref.3) were confirmed.

2) There is no benefit from the vortex flap at incidences higher than the stalling incidence.

3) The highest value of $(L/D)_{max}$ is achieved using a modest flap deflection angle with the wing at, or close to, the rather small incidence for which the flow comes smoothly onto the flap.

4) At incidences higher than in 3), the L/D reaches a local maximum when the vortex flap is deflected so that a leading-edge separation vortex is formed on the LEVF top surface with the reattachment line coincident with the flap hinge line, (as was suggested in ref.1). However this 'local' value of $(L/D)_{max}$ is smaller than that in 3).

5) The L/D ratio of the basic wing (no LEVF) is improved by incorporating a parallel vortex plate, especially when the plate protrudes ahead of the leading-edge of the wing. The improvement measured here was comparable to that obtained from a LEVF deflection of 30°.

6) The tapered vortex flap with or without the LEVF deflected showed no significant improvement in L/D ratio.

7) There is very little change of pitching moment for any of the leading-edge devices tested here.

References

1) Rao, D.M., "Leading Edge Vortex-Flap Experiments on a 74deg. Delta wing," NASA CR-159161, 1979.

2) Campbell, J.F. and Osborn, R.F., "Leading-Edge Vortex Research: Some Nonplanar Concepts and Current Challenges," NASA CP-2416, 1986, pp.31-63.

3) Stollery, J.L. and Ellis, D.G., "The Behaviour and Performance of Leading-Edge Vortex Flaps," ICAS-88-4.5.2, 1988, pp.758-765.

4) Rao, D.M. and Johnson Jr., T.D., "Investigation of Delta Wing Leading-Edge Devices," *J. Aircraft*, Vol.18, March 1981, pp.1051-1056.

5) Rinoie, K. and Stollery, J.L., "Experimental Studies of Vortex Flaps and Vortex Plates Part.1 0.53m Span 60deg Delta Wing," College of Aeronautics Report No.9113, Cranfield, Aug. 1991.

6) Rinoie, K. and Stollery, J.L., "Experimental Studies of Vortex Flaps and Vortex Plates Part.2 1.15m Span 60deg Delta Wing," College of Aeronautics Report No.9205, Cranfield, March 1992.

7) Jaquet, B.M. and Brewer, J.D., "Low-Speed Static-Stability and Rolling Characteristics of Low-Aspect-Ratio Wings of Triangular and Modified Triangular Plan Forms," NACA RM No.L8L29, 1949.

8) Jones, R., Miles, C.J.W. and Pusey, P.S., "Experiments in the Compressed Air Tunnel on Swept-back wings including two delta wings," A.R.C. Tech. Report R.& M. No.2871, 1954.

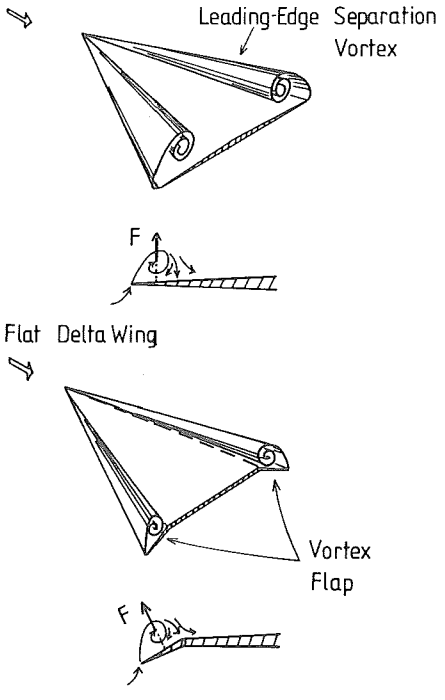

Fig.1 Concept of Vortex Flap

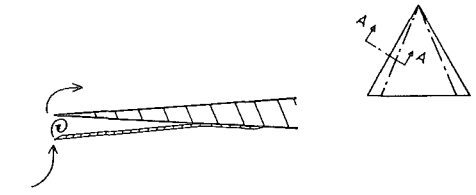

a) Flat Delta Wing with Vortex Plate

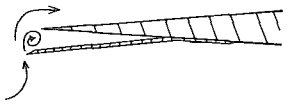

b) Flat Delta Wing with Protruding Vortex Plate

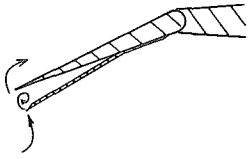

c) Delta Wing with Vortex Plate when LEVF is deflected

Fig.2 Concept of Vortex Plate

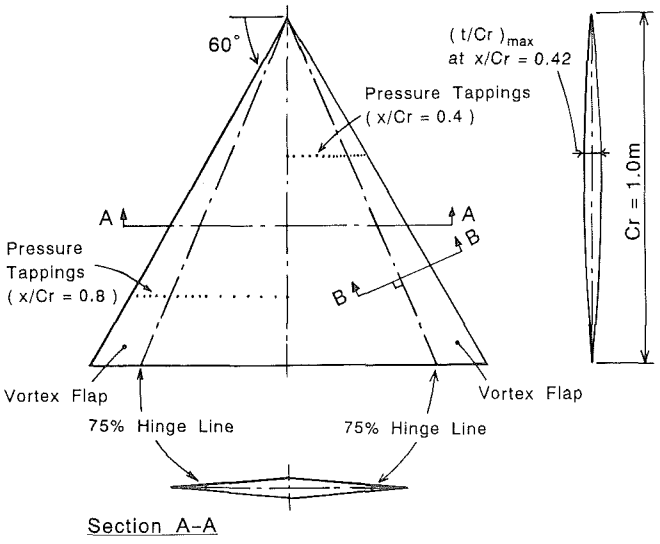

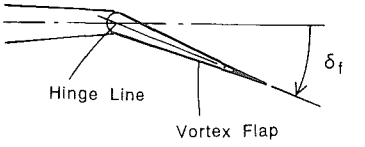

Section B-B with Vortex Flap deflected

Fig.3 Delta Wing Model with LEVF

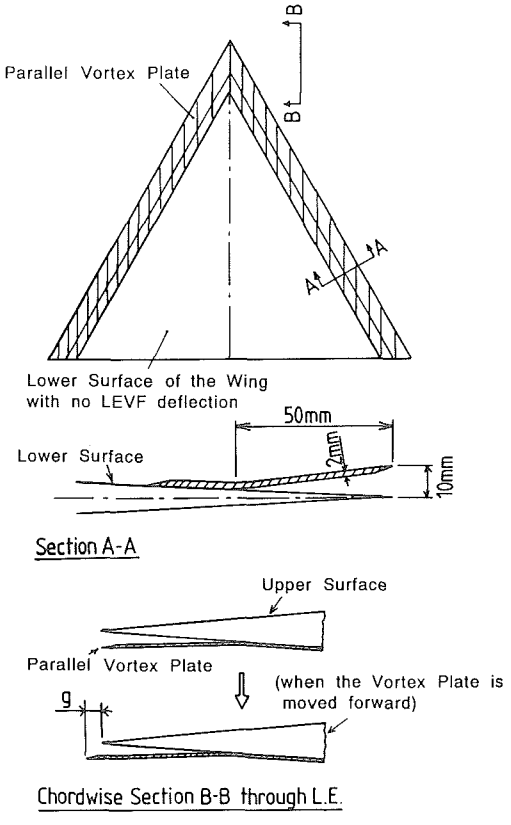

a) Parallel Vortex Plate

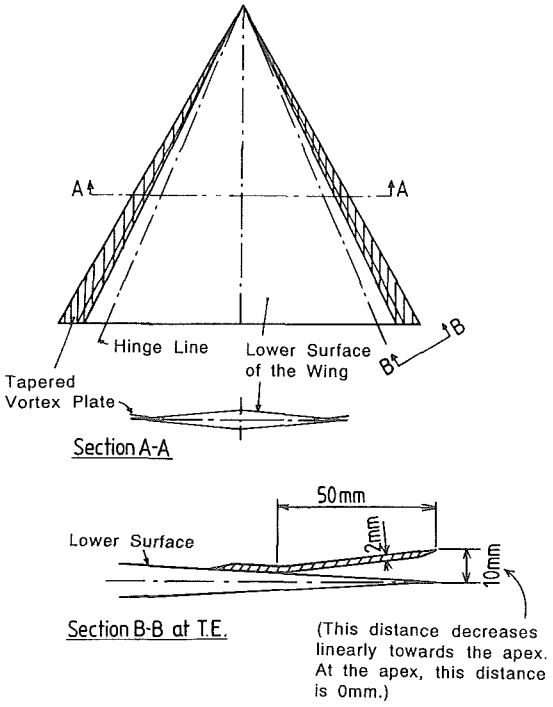

b) Tapered Vortex Plate

Fig.4 Delta Wing Model with Vortex Plate

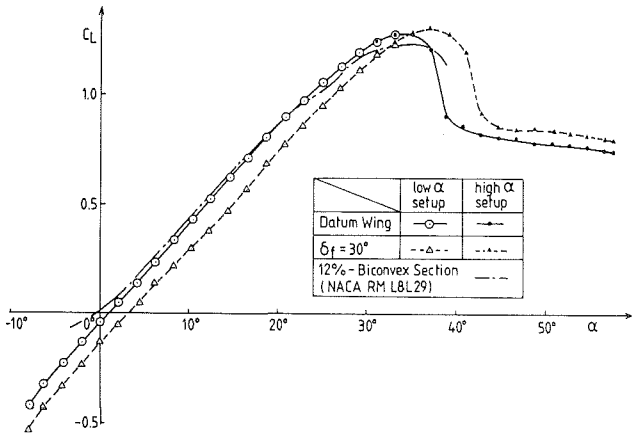

Fig.5 Effect of LEVF on C_L vs. α

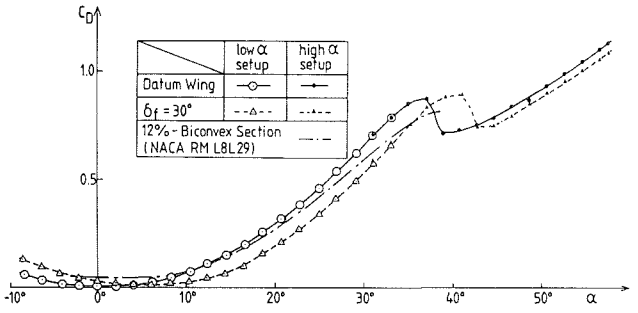

Fig.6 Effect of LEVF on C_D vs. α

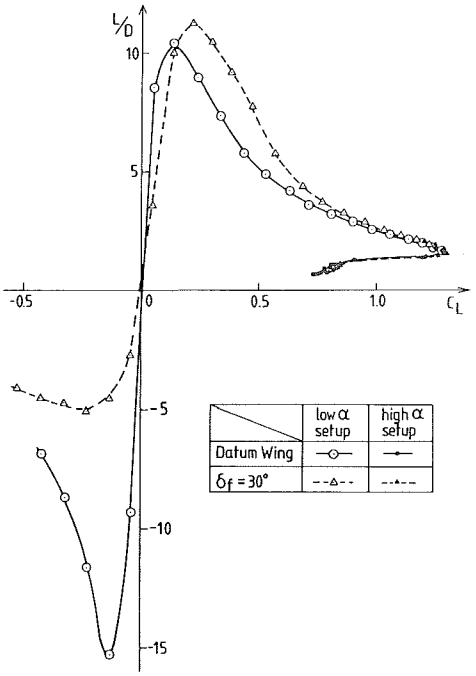

Fig.7 Effect of LEVF on L/D vs. C_L

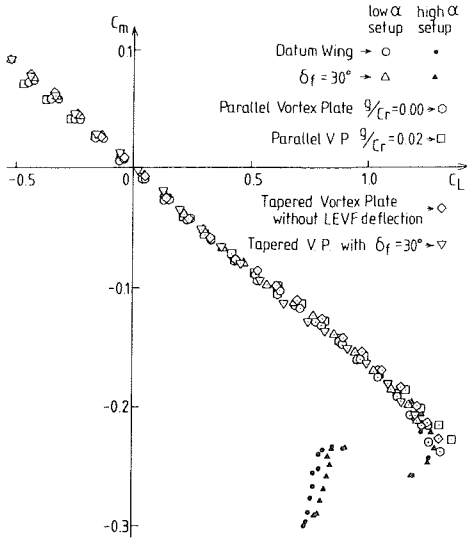

Fig.8 Effect of LEVF on C_m vs. C_L

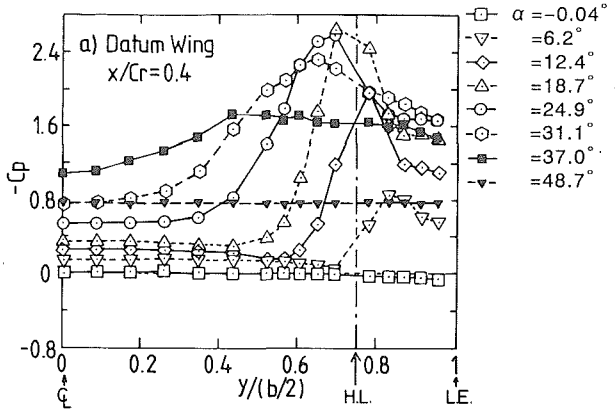

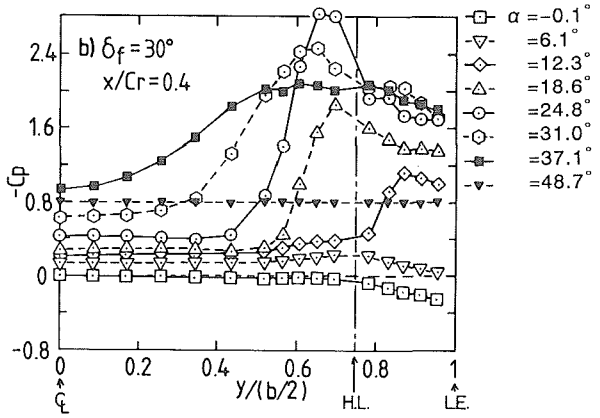

Fig.9 Surface Pressure Distributions for Datum Wing and $\delta_f = 30°$ at $x/C_r = 0.4$

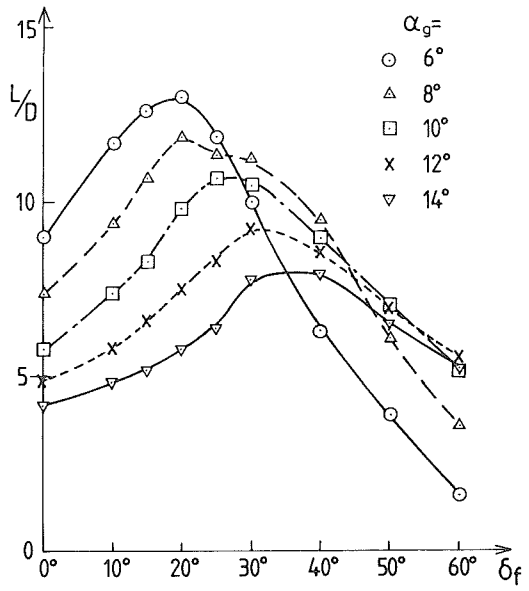

Fig.10 L/D vs. δ_f at Constant α_g

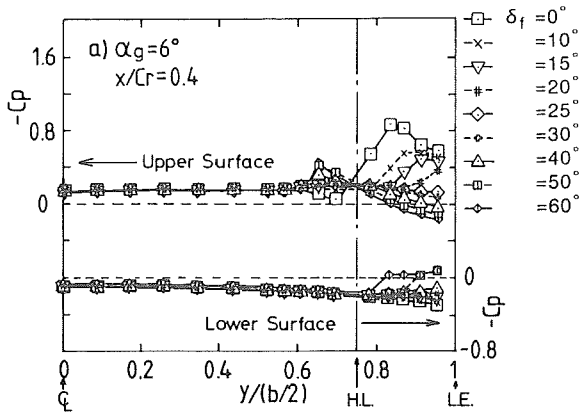

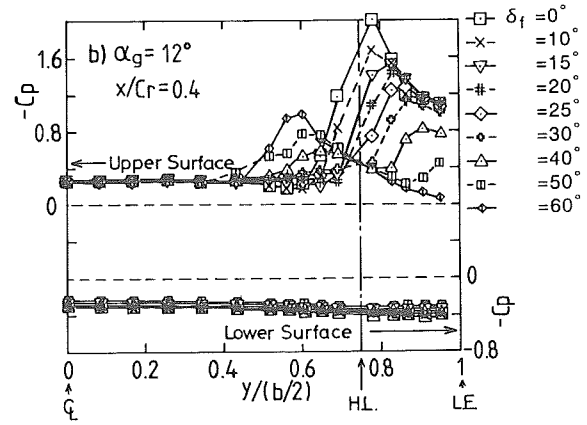

Fig.11 Surface Pressure Distributions at Constant Incidence for $\alpha_g = 6^\circ$ and 12° at $x/Cr = 0.4$ (Upper & Lower Surface)

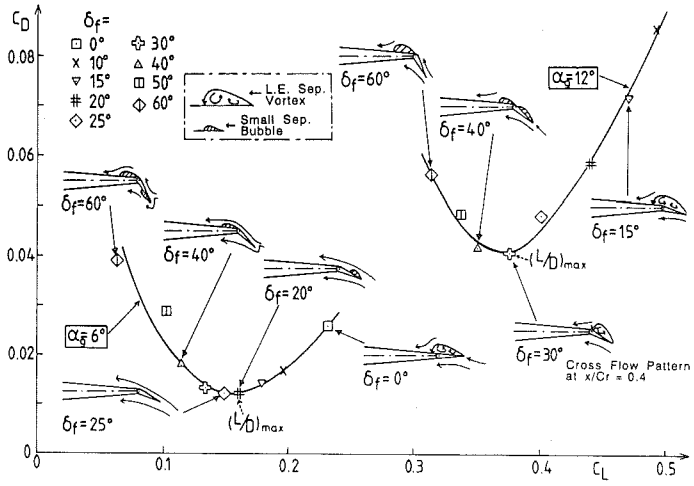

Fig.12 C_D vs. C_L and Cross Flow Patterns at $\alpha_g = 6^\circ$ & 12°

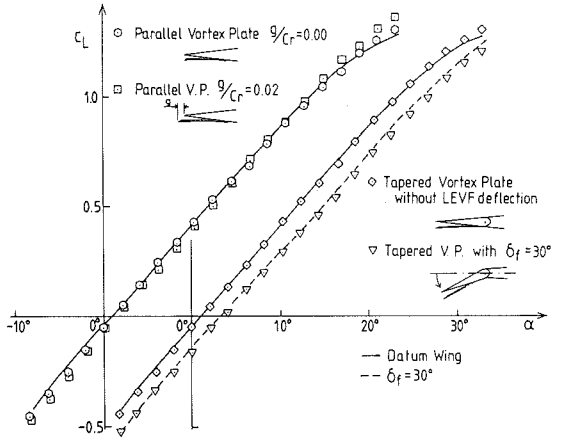

Fig.13 Effect of Vortex Plate on C_L vs. α

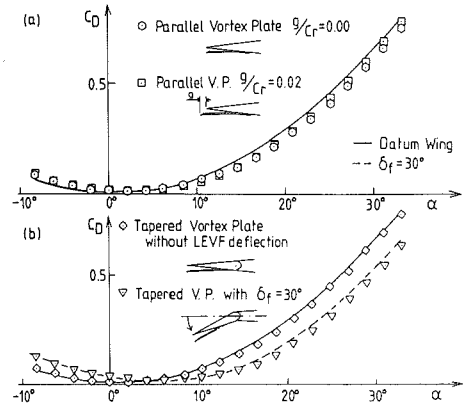

Fig.14 Effect of Vortex Plate on C_D vs. α

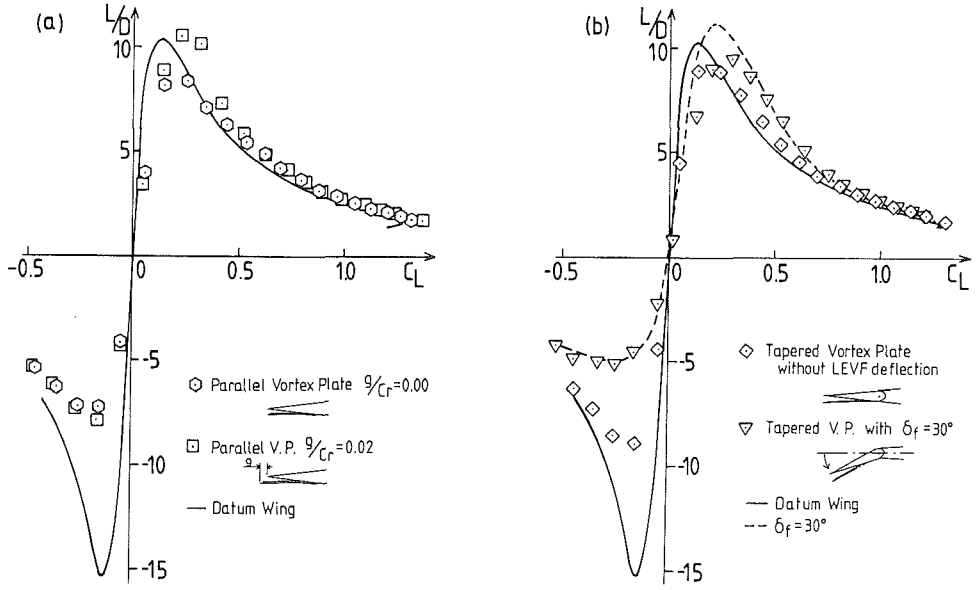

Fig.15 Effect of Vortex Plate on L/D vs. α

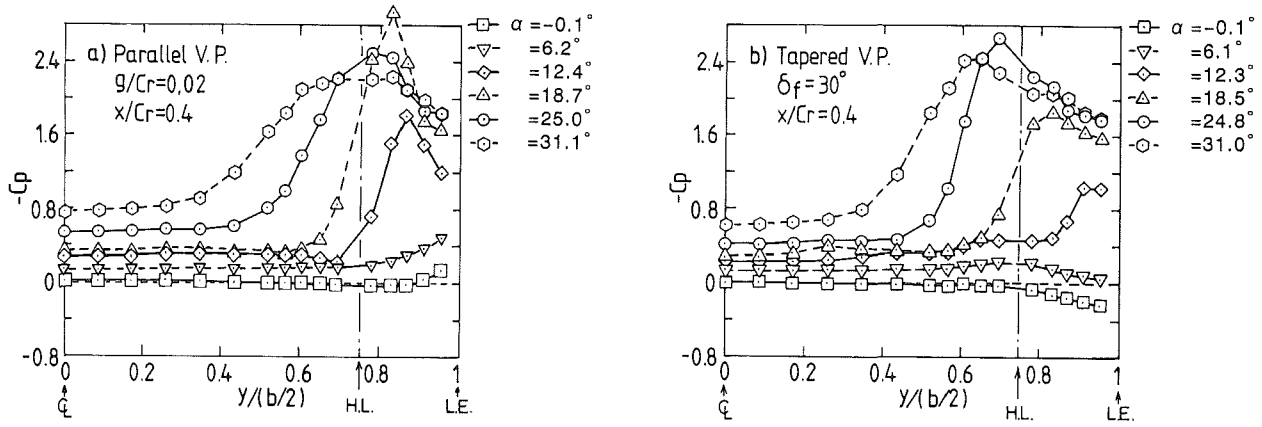

Fig.16 Surface Pressure Distributions at $x/Cr = 0.4$ for Parallel Vortex Plate $g/Cr = 0.02$ and for Tapered Vortex Plate with $\delta_f = 30°$ deflection

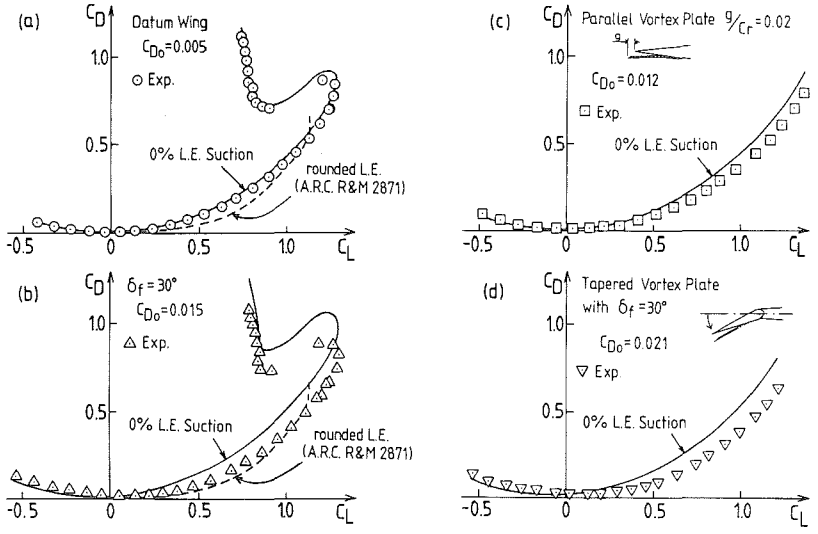

Fig.17 Effect of Leading-Edge Suction Force on C_D